Mineral equilibria at high PT-parameters

Gnuchev Y.Y., Bychkov D.A., Koptev-Dvornikov E.V. A single olivine liquidus compositometer for water-containing and anhydrous systems. *UDC 553.212, 552.111*

Russian Federation, Moscow, GSP-1, Leninskie Gory, Lomonosov Moscow State University, Geological Faculty, 119234 gnuchevyy@my.msu.ru, dmibychkov@gmail.com, ekoptevmail@gmail.com

Abstract: Based on the MELT database provided by A.V. Girnis, a sample of water-saturated, water-containing and nominally anhydrous experiments reproducing the olivine-melt equilibrium was formed, containing the results of 1885 quenching experiments characterizing silicate systems in a wide range of intensive parameters.

As a result of optimization, an olivine compositometer was obtained, (a system of equations) reproducing the content of the main minerals with an accuracy of no worse than ± 0.5 mol. % 95% confidence level for all experiments in both dry and water-containing systems.

The compositometer was verified by comparing the calculated and experimental pressures and temperatures of olivine liquidus. The width of the confidence interval for temperature estimation with a 95% probability does not exceed ±2.5 °C. The average deviations of the calculated concentrations of minerals from the experimental ones do not exceed 0.04% by weight, which indicates that the estimate is not biased.

Keywords: *olivine compositometer, thermobarometer, experimental sampling, silicate melt, thermodynamic equilibrium*

Our research group has currently developed a set of compositometers (Aryaeva et al., 2016; Bychkov 2024; Koptev-Dvornikov et al., 2012, 2019, 2020; Romanova et al., 2020) that can predict the crystallization of olivine, plagioclase, augite, orthopyroxene, and ore minerals (sulfides, chromospinels, magnetite, and ilmenite) coexisting with melt. However, these equations were derived by processing the results of anhydrous experiments, whereas the vast majority of natural magmas and lavas are hydrous to a greater or lesser extent.

Experimental studies demonstrate that the presence of water in the melt causes a significant but differentiated decrease in mineral crystallization temperatures.

Olivine thermobarometer developers often fail to consider the effect of water concentration on the composition of crystallizing olivine. We decided to develop a universal olivine compositometer (a system of equations for calculating the compositions of minerals in equilibrium with a melt), applicable to both nominally anhydrous and hydrous and water-saturated systems, allowing us to calculate the liquidus temperature and composition of olivine over the entire range of melt water contents.

Initial attempts to optimize an equation of the type (Bychkov et al., 2007) for olivine end members yielded suboptimal results. However, earlier, during the development of an equation for calculating the saturated melt water content (Gnuchev et al., 2023; Gnuchev et al., 2025), a similarity between the equation's form and the compositometer's form was noted.

The compositometer form we adopted, after trying several options, takes into account the dependence of the reaction volume effect (β) on melt composition. The resulting equation is represented as follows (1):

$$X_m^j = \exp\left[\frac{A_m^j + \beta_m^j(X)P}{T} + B_m^j(X) + \sum_{i=1}^{n} \nu_{m,i} \ln a_i^l\right] \quad (1)$$

$$\beta_m^j(X) = \beta_{m,0}^j + C_{m,\beta}^j \frac{X_{MgO} * X_{HO_{0.5}}}{X_{SiO_2}} + D_{m,\beta}^j \lg fO_2 + \sum_{i=1}^{n} \beta_{m,i}^j X_i$$

$$B_m^j(X) = B_{m,0}^j + C_{m,B}^j \frac{X_{MgO} * X_{HO_{0.5}}}{X_{SiO_2}} + D_{m,B}^j \lg fO_2 + \sum_{i=1}^{n} B_{m,i}^j X_i,$$

when $B_{m,0}^j$ и $b_{m,0}^j$ - constants, $C_{m,b}^j$, $C_{m,B}^j$, $D_{m,b}^j$, $D_{m,B}^j$, $b_{m,i}^j$, $B_{m,i}^j$ - coefficients of the corresponding variables, X_{MgO}, $X_{HO_{0.5}}$, X_{SiO_2} - mole fractions of melt components; X_m^j – mole fraction of the j-th end member of any crystalline phase *m*; P – kbar; T – absolute temperature; fO_2 – oxygen fugacity in bars, $W=\ln((Na+K)*Al/Si^2)$, X_i^l – mole fraction of the i-th component of the melt, n – number of components taken into account, $n_{i,m}$ - stoichiometric coefficient in the reaction of minal formation *m*, a_i^l - activity of component i in the melt, calculated according to the Nielsen–Dungan two-lattice model (Nielsen, Drake, 1979; Nielsen, Dungan, 1983). *A, β, D, E, F, J* – coefficients of the corresponding variables, B – constant.

Finding the coefficients for the variables (optimization) was performed by minimizing the squares of the differences between the calculated and experimental contents of the end-members.

Expressions similar in meaning to equation (1) are traditionally called thermobarometers in the literature.

We used this form of the equation to find the coefficients during optimization of the system of equations in the olivine compositometer.

The optimization was based on a sample we compiled. The primary data source for the sample was the MELT database (Girnis 2023).

The final sample, after optimization of the system of equations, consisted of 1885 experiments and is presented below.

The polyhedron in the coordinates of oxide concentrations for the newly formed sample is characterized by the following values of wt.% (oxide content in the melt, recalculated to an anhydrous basis): SiO_2 from 40.2 to 66.8, TiO_2 from 0 to 6.8, Al_2O_3 3.3–22.3, FeO* 3.2–30.5 (FeO* - all iron, recalculated to FeO), MgO 1.5–21.0, CaO 1.9–18.7, Na_2O 0.0–9.72, K_2O 0–6.7, H_2O 0–10.8. The experiments were performed in the temperature range from 1200 to 1700 K and pressures from 1 bar to 15.0 kbar.

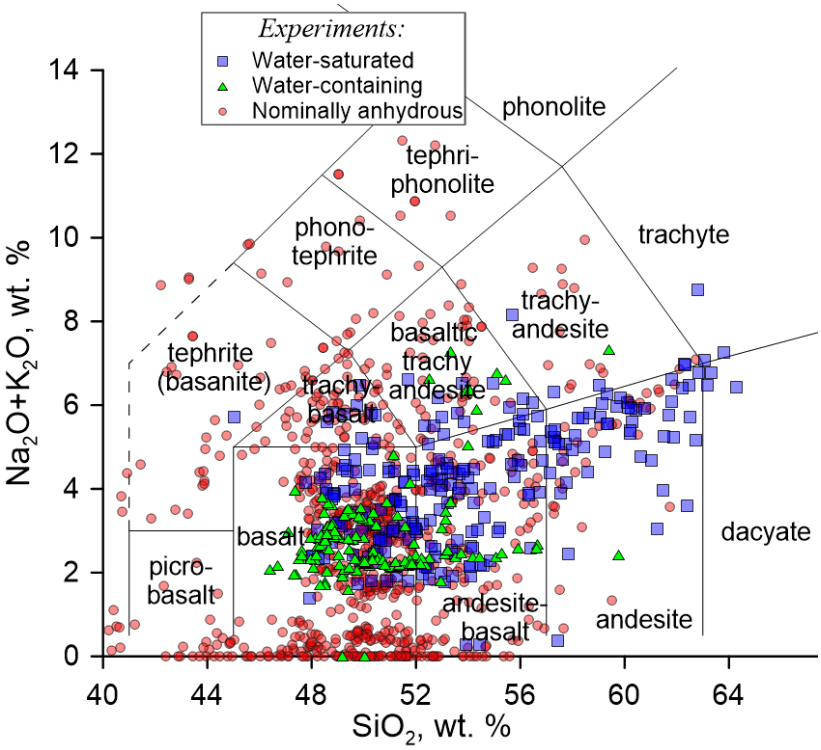

Fig. 1 TAS diagram. Range of variation of experimental melt compositions in the final sample (1885 experiments).

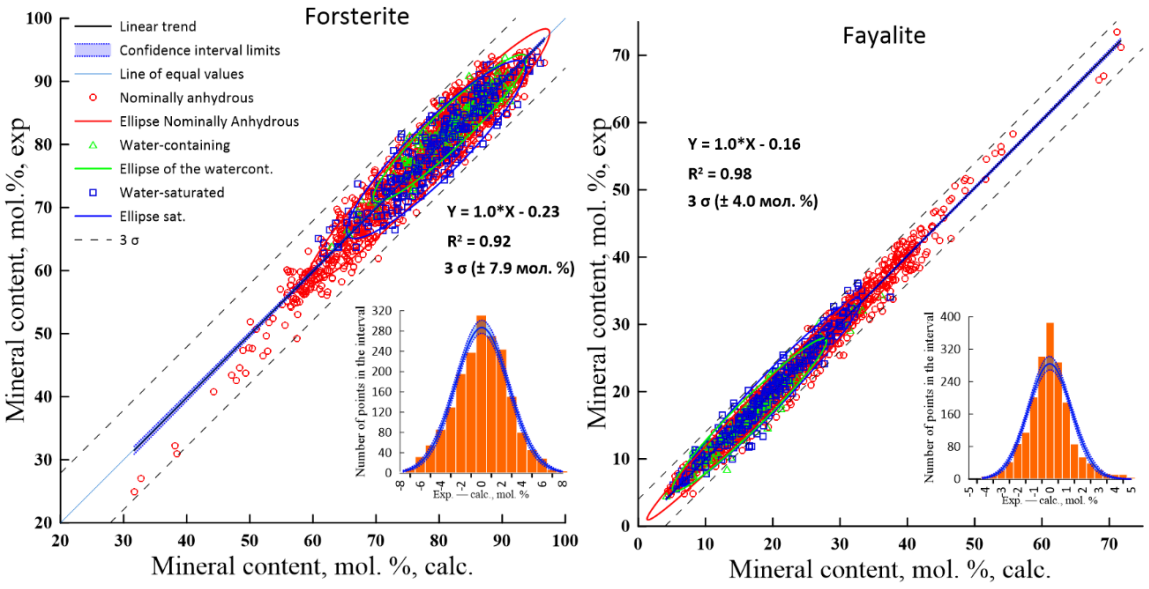

Fig. 2. Comparison of calculated forsterite and fayalite contents with experimental data. The black line is the linear trend, the blue dotted line is the line of equal values. The blue translucent area is the confidence region at the 95% confidence level, 1885 experiments in the sample.

Results of optimization of olivine compositometer coefficients

The results of the olivine compositometer optimization are presented in Figure 2.

The graphs include scatter ellipses to illustrate the distribution of points for three subsets—nominal anhydrous, hydrous, and hydrous experiments. The ellipse boundaries correspond to 2 σ, meaning the

probability of a point falling within the ellipse is 86%.

The graphs demonstrate high-quality prediction of forsterite and fayalite concentrations across the entire range of melt compositions, water contents, and pressures. The shape of the residual histograms is close to a normal distribution, allowing deviations from the calculated values to be considered random and the use of statistical tools to assess the quality of the approximation. The maximum confidence band at the 95% confidence level is ±0.5 mol% for forsterite and ±0.3 mol% for fayalite.

Verification of olivine compositometer

The essence of verification is that, for a given melt composition, oxygen fugacity, and pressure, an iterative method is used to find the temperature at which the sum of the mole fractions of the end-members in olivine equals unity. This temperature is then taken as the calculated liquidus temperature of olivine. It should be emphasized that this verification stage characterizes not the quality of each equation in the compositometer system, but the result of their combined solution.

Figure 3 shows the correlation between the experimental and calculated liquidus temperatures for the entire olivine sample, along with the corresponding histogram of the residual distribution. Comparison of the experimental and calculated liquidus temperatures demonstrates high accuracy of reproduction: the line of equal values lies within the confidence region, and its maximum width is ±2.5°C.

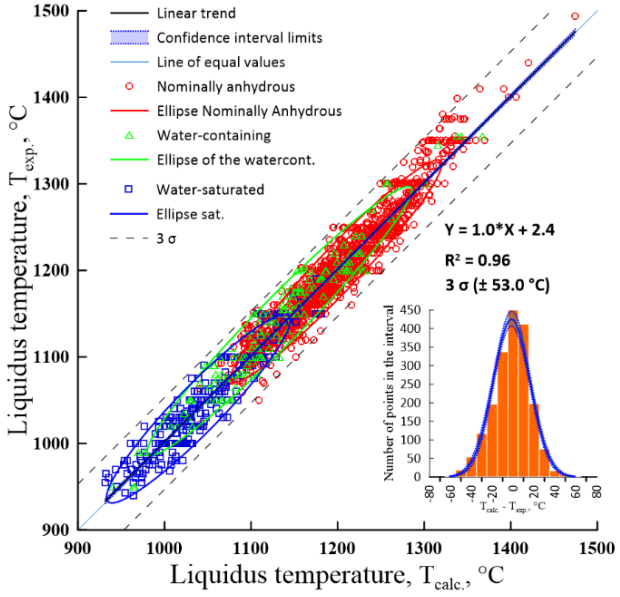

Fig. 3. Correlation between experimental and calculated values of olivine-melt liquidus temperature for a sample of 1356 experiments, and the corresponding histogram of the distribution of residues.

Conclusions

The final experimental data set, including nominally anhydrous, hydrous, and hydrous experiments, comprised 1885 experiments.

The consistent orientation of the ellipses' axes in the graphs in Figures 2 and 3 indicates that we have succeeded in developing an equation that is truly unified for all three subsets.

The developed olivine compositometer accurately reproduces olivine compositions and mineral crystallization liquidus temperatures over a compositional range from basalt to andesite.

Funding: This study was conducted as part of a government assignment to Lomonosov Moscow State University.

Acknowledgments: *We would like to thank A.V. Girnis for providing the MELT database.*

References

1 Aryaeva N. S., Koptev-Dvornikov E. V., Bychkov D. A. (2012) Thermobarometer equation for describing sulfide-silicate liquation in mafic systems. Petrology. 20 (5), 495–495.

2 Bychkov D. A. (2024) CriMinal program and a set of compositometers: tools for modeling silicate melt–mineral equilibrium, Diss. Cand. of Geol.-Min. Sci. (2018). Moscow: Lomonosov Moscow State University, Geological Faculty, 139 p.

3 Girnis A. V. (2023) Distribution of rare elements between olivine and melt: generalization of experimental data. Geochemistry. 68 (4), 327–340.

4 Gnuchev Ya. Yu., Bychkov D. A., Koptev-Dvornikov E. V. (2023) New version of the equation for calculating saturated water contents in silicate melts. Geochemistry. 68 (9), 926–937.

5 Gnuchev Ya. Yu., Bychkov D. A., Koptev-Dvornikov E. V. (2025) Recalibration of the equation for calculating the water content in silicate melt–aqueous fluid equilibrium. Geochemistry. 70, No. 8, pp. 71–82.

6 Koptev-Dvornikov E. V., Aryaeva N. S., Bychkov D. A. (2012) Thermobarometer equation for describing sulfide-silicate liquation in basic systems. Petrology. 20(5), 495-495.

7 Koptev-Dvornikov E.V., Bychkov D.A. (2019) Development of a liquidus thermobarometer for modeling olivine-melt equilibrium. Moscow University Bulletin. Series 4: Geology. (5), 62-74.

8 Koptev-Dvornikov, E.V., Bychkov, D.A. (2007). Geothermometers for a wide range of basite compositions. Irkutsk: SB RAS, 178-181

9 Koptev-Dvornikov E.V., Romanova E.S., Bychkov D.A. (2020) Orthopyroxene thermobarometer-composiometer for the composition range from magnesian basites to dacites. Proceedings of the All-Russian Annual Seminar on Experimental Mineralogy, Petrology, and Geochemistry, 74-77.

10 Romanova E.S., Koptev-Dvornikov E.V., Bychkov D.A. (2020) Pigeonite liquidus thermobarometer for the melt composition range from magnesian basites to dacites. Proceedings of the All-Russian Annual Seminar on Experimental Mineralogy, Petrology, and Geochemistry, 90-93.

11Nielsen, R. L., Drake, M. J. (1979) Pyroxene-melt equilibria. Geochim. Cosmochim. Acta. 43(8), 1259-1272.
12 Nielsen, R. L., Dungan, M. A. (1983) Low pressure mineral-melt equilibria in natural anhydrous mafic systems. Contrib. Mineral. Petrol. 84(4), 310-326.

Kostyuk A.V.[1], Vasyukova O.V.[2], Serdyuk A.A.[1], Williams-Jones A.E.[2] Experimental modeling of the genesis of alkaline silicate melts using the silicate-carbonate system at 800-1000°C, 200 MPa. *UDC 550.4.02*

[1] IEM RAS, Chernogolovka, Russia, nastya@iem.ac.ru
[2] McGill University, Montreal, Canada

Abstract. The current view on the origin of carbonatite complexes suggests that the alkali silicate rocks within them are fractionation products of carbonated alkaline-ultramafic magma, alkali silicate rocks, and, ultimately, carbonatites. However, alternative hypotheses exist that suggest that carbonatite magmas, with their very low viscosity, can percolate through host rocks, interact with them, and metasomatically alter them. To model this scenario, a series of experiments were conducted to study the interaction of silicate glass with Na_2CO_3-bearing dolomite liquid at temperatures of 800–1000°C and a pressure of 2 kbar using the high-pressure gas facility at the IEM RAS.

Keywords: *carbonatites, alkaline silicate melts, experiment*

Carbonatite complexes are the source of the largest deposits of important minerals, particularly rare elements (niobium, tantalum, and rare earth elements), as well as other valuable minerals such as zirconium, phosphorus (apatite), and iron. Carbonatites are typically associated with alkali silicate and ultramafic rocks.

The idea that the mantle is metasomatised by dolomitic magmas (wehrlitisation) was proposed decades ago and is widely accepted as a means of providing armoured conduits for the ascent of these magmas into the crust. According to this hypothesis, dolomitic magma reacts with orthopyroxene in the mantle to produce a layer of olivine plus clinopyroxene (wehrlite), thereby providing an inert pathway for the ascent of subsequent batches of magma. The question that has not been fully addressed is what happens when carbonatitic magmas encounters continental crust.

To investigate the interaction of dolomitic liquid (alkali-bearing) with continental crust, we conducted experiments at 800-1000ºC and 2 kbar using the high-pressure gas facility. The continental crust was represented by silicate glass having the composition of granitic gneiss (Glass 1) and sodic fenite (Glass 2). A schematic representation of the ampoule assembly and longitudinal sections of samples after experiments are shown in Fig. 1.

The experimental products were studied on a Tescan Vega II XMU digital scanning microscope with an energy-dispersive X-ray spectrometer (EDS) with an INCA Energy 450 semiconductor Si (Li) detector and an INCA Wave 700 wave-dispersive spectrometer (WDS) in Energy Plus mode. Detection limits with a 95% probability are equal to 2σ. The analytical results were processed using INCA ver. 4.06 and Atlas software at the IEM RAS.

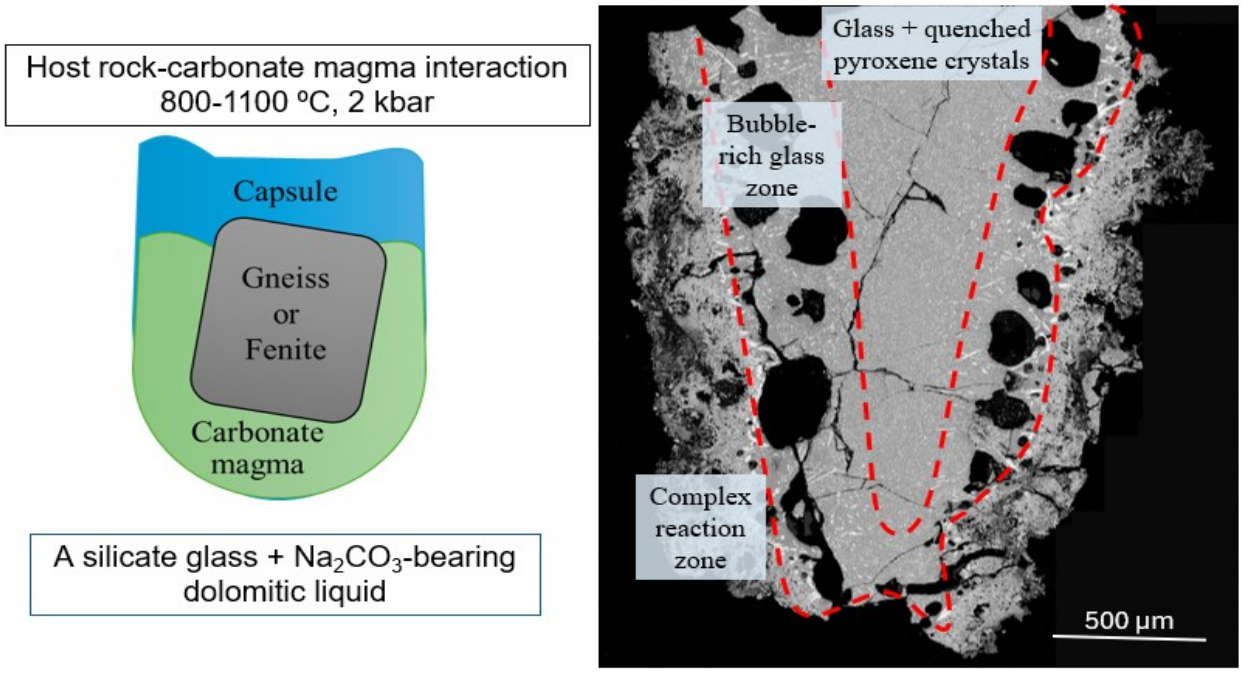

Fig. 1. Schematic representation of the assembly of the experimental ampoule (a) and BSE micrographs of longitudinal sections of samples (b) after experiments in the silicate glass-carbonate melt system.

All the experiments produced a rind on the glass comprising the following zones:

1) an innermost alkali silicate melt quenched to silicate glass (phonolite);

2) nepheline and aegirine-augite (ijolite);

3) fine-grained diopside, olivine, phlogopite and calcite (pyroxenite or glimmerite); and

4) an outermost coarse-grained calcite carbonatite containing phlogopite and olivine (Fig 2).

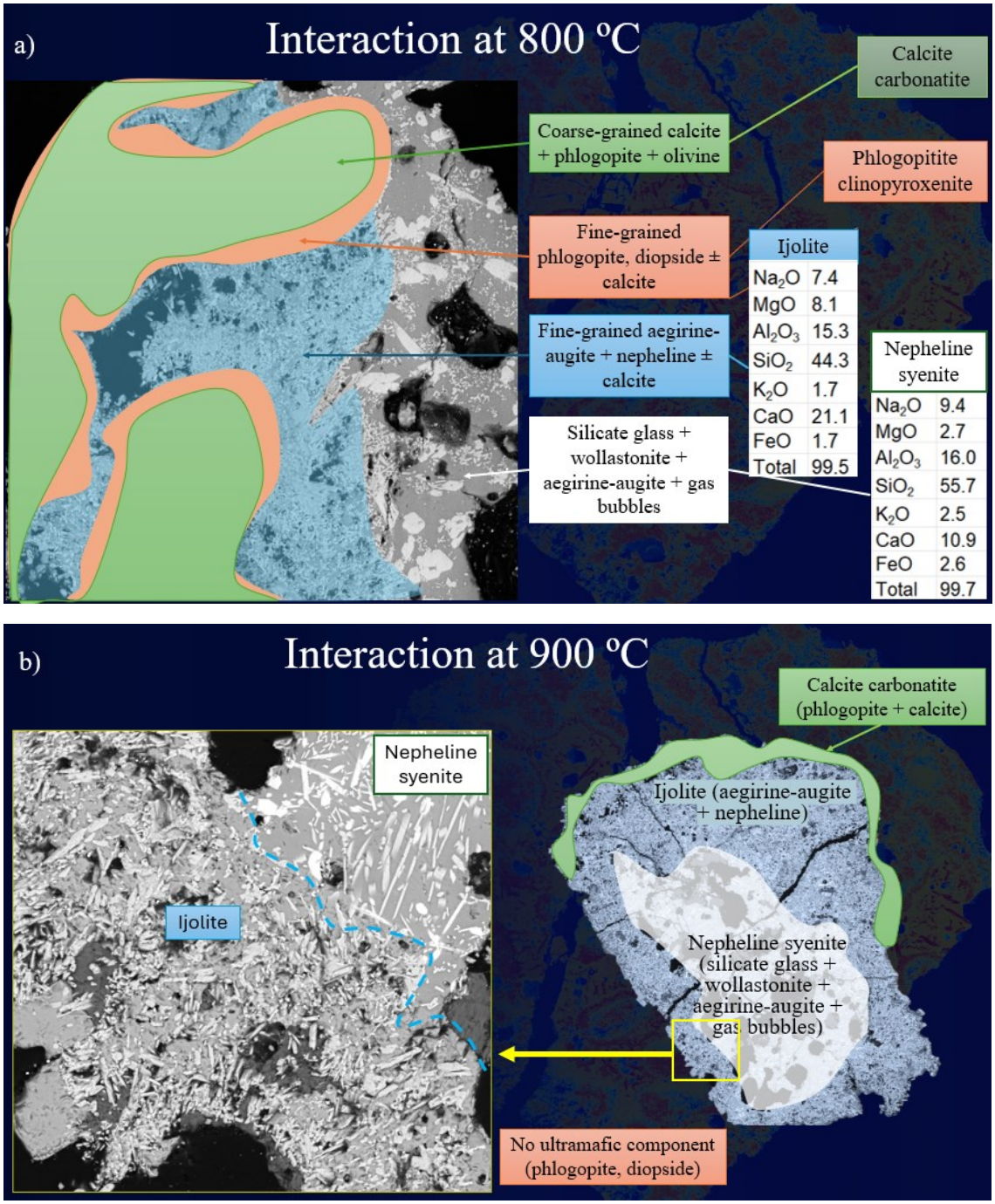

Fig. 2. BSE Micrographs of polished surfaces of samples with the application of zoning boundaries in the reaction rim after experiments at 2 kb and (a) 800°C, (b) 900 °C in the silicate glass-carbonate melt system.

Zones 1 and 2 are interpreted to be products of melting of the glass induced by a Na-enriched carbonate liquid. Zone 3 is the product of the metasomatic alteration of the glass by Mg- and Ca-rich carbonate liquid. Zone 4 crystallised from the carbonate liquid, which assimilated silicate components from the glass. The proportions of the zones varied with temperature and the composition of the glass; pressure had a major effect on the generation of Zones 1 and 2 (Fig 3).

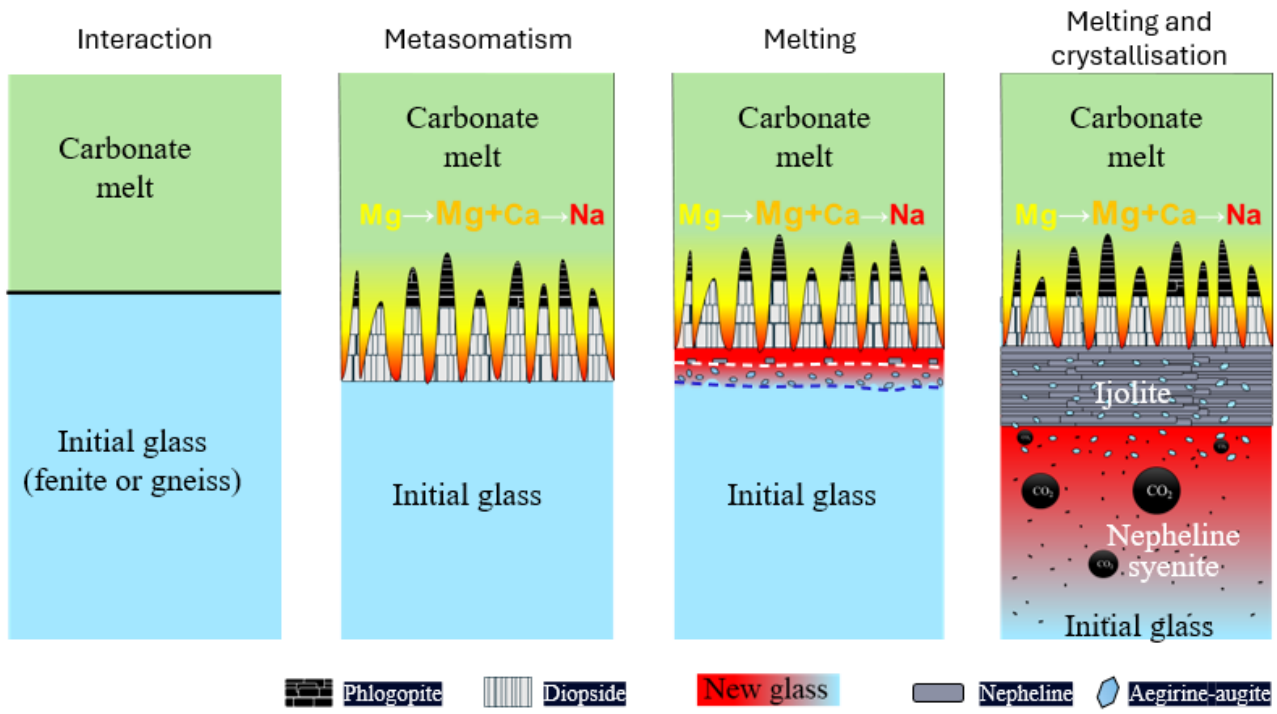

Fig. 3. Schematic representation of the formation of a reaction zone during the interaction of carbonate melt with glass (gneiss).

The interaction of carbonatitic magmas with the continental crust armours the magma conduits in a manner similar to that in which the mantle is wehrlitised, but more extensive than in the mantle due to the higher Si chemical potential gradient in the continental crust. This explains the common occurrence of ultramafic and/or alkaline silicate rocks in carbonatite complexes and their relative proportions.

This study is fulfilled under Research program № FMUF-2022-0001 of the Korzhinskii Institute of Experimental Mineralogy.

Kostyuk A.V., Gorbachev N.S., Novikov M.P., Nekrasov A.N. Influence of fluid on metal-sulfide liquation of FeS-Fe-C melt in the basalt-sandstone system at 1250°C, 300 MPa. *UDC 550.4.02*

IEM RAS, Chernogolovka, nastya@iem.ac.ru

Abstract. Experiments at 1250°C and 300 MPa were conducted under dry and oil-saturated conditions in a basalt-sandstone system. All experiments were conducted in platinum ampoules using graphite containers at a high-pressure gas rig at the Institute of Experimental Mineralogy, Russian Academy of Sciences. Powders of ground Mokulaev basalt and pyrite-bearing sandstone from the Norilsk region were used as starting materials. Sulfur-containing oil was used as the source of the C-O-H-S fluid. Following the experiments, changes in the phase composition of samples with varying degrees of melting and the ratios of coexisting liquids were observed. The phase composition and trace element concentrations in the sulfide, metallic, and silicate melts indicate the important role of fluid in the genesis of sulfide-metal mineralization.

***Keywords**: basalt, sulphide, sandstone, contamination, experiment, fluid*

Contamination of basaltic magma with sedimentary rocks dramatically alters the physicochemical equilibrium of the system, triggering the dissolution of the sedimentary strata, the transport and exchange of both petrogenic and ore elements, changes in redox conditions, saturation with volatile components, and, consequently, the process of sulfide liquation (Grinenko, 1984; Iacono-Marziano et al., 2017; Barnes et al., 2023; Kostyuk et al., 2025). Sulfide liquid, separating from silicate magma, concentrates chalcophile elements (Ni, Cu, Co, PGE), thereby changing the composition of the remaining magma and accumulating ore elements in giant sulfide deposits, such as those at Norilsk.

In this paper, we present the results of an experimental study of the interaction of basaltic magma with host rocks using the example of a basalt-pyrite-containing sandstone system under dry and fluid-containing conditions at 300 MPa, 1250°C.

Experiments were conducted using a quenching technique in platinum ampoules with internal graphite containers at the IEM RAS facilities. Mokulaevsky basalt glass was used as the starting composition (wt.%): SiO_2 – 50.02, TiO_2 – 1.85, Al_2O_3 – 14.51, FeO – 14.03, MgO – 5.85, CaO –

10.40, Na_2O – 2.50, K_2O – 0.72. A sandstone sample with inclusions of carbonaceous matter and pyrite (Py) was used as the contamination material. To simulate contamination of basaltic melt with sulfide-, oil-, and gas-containing rocks, S-containing petroleum hydrocarbons (hereinafter referred to as oil) were used as the source of C–O–H–S fluid. This oil sample from the Volga-Ural oil and gas basin contained 3.9 wt.% S, 18 mg/kg Ni, and 108 mg/kg V (Lakhova et al., 2022).

Oil (5% by weight) was mixed with sedimentary rock powder and placed in the center of the sample. The starting compositions were loaded layer by layer into a graphite container, tightly sealed with a lid, then placed in a platinum ampoule and sealed. Oxygen fugacity under the given conditions corresponded to a C–CO–CO_2 buffer.

The experimental products were studied using a Tescan Vega II XMU digital scanning microscope equipped with an INCA Energy 450 energy-dispersive X-ray spectrometer (EDS) and an INCA Wave 700 wave-dispersive spectrometer (WDS) in Energy Plus mode at the Institute of Experimental Mineralogy, Russian Academy of Sciences.

Below is a description of the phase and chemical compositions of the samples after experiments in dry and C–O–H–S-containing basalt-sandstone systems at 300 MPa and 1250°C.

In the basalt-sandstone system, under dry conditions, the sample retains traces of its original texture, with a visible boundary between the sandstone (center) and basalt (upper and lower parts of the section) (Fig. 1a). The basalt zone is composed of well-tempered glass of andesite-basalt composition (L). After melting and interaction with basalt, the sandstone forms a narrow zone composed of a refractory residue of numerous quartz grains (Qz) cemented by intergranular silicate glass (L_2) of alkali-dacite composition. This zone also contains both individual large and smaller drop-shaped segregations of the Fe–S sulfide fraction.

In the basalt–sandstone–oil system, the original structure of the sample with clear boundaries between the basalt and the rock was preserved in the longitudinal section after the experiment. The central part of the sample is composed of large quartz grains (Qz) up to 200 μm in size, cemented by an acidic melt of rhyolitic composition (L_2). The basaltic melt (L) after interaction with sandstone is a homogeneous glass of andesitic composition (Fig. 1b, Table 1), along the boundary of which and at the contact with the rock, sulfide-metal droplets are observed (Figs. 1b, 2b).

In both systems, melting of the sedimentary rock was accompanied by the dissolution of the original pyrite, the formation of a sulfide Fe–S–C melt, and its subsequent stratification into Fe–metallic and Fe–sulfide melts. Under dry conditions, multiple small sulfide phases of Fe–S composition ranging in size from a few to 10 μm, as well as single large ones 50–100 μm in size (Fig. 2a), were concentrated in the central zone of the sandstone (Fig. 1a). The metallic phase is present only in the largest sulfide droplets in the form of small veinlets (Fig. 2a) with a Ni concentration of up to 4 wt.% (Table 2).

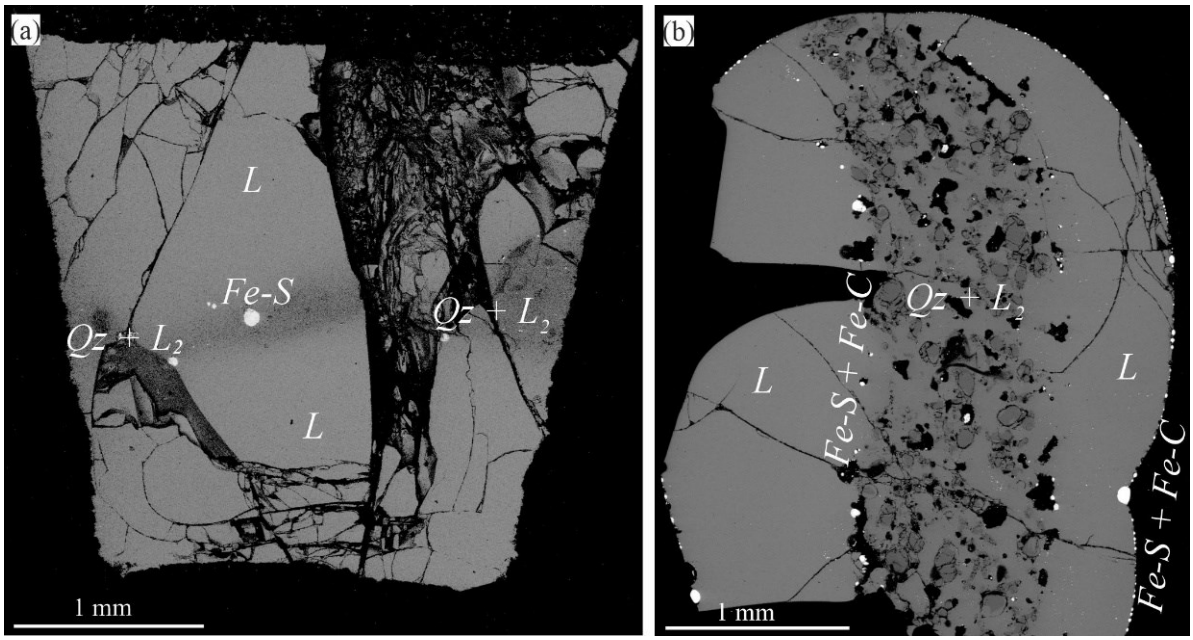

Fig. 1. Backscattered electron micrographs of longitudinal sections of samples after experiments in the basalt-sandstone system: a) in dry conditions, b) in the presence of C–O–H–S fluid.

Table 1. Chemical compositions (wt.%) of silicate melts after experiments in basalt – sandstone ± oil systems at 1250°C, 300 MPa.

Phase	SiO_2	TiO_2	Al_2O_3	FeO	MgO	CaO	Na_2O	K_2O	SO_3	Sum
dry conditions										
***L*, *n* = 18**	54.14 ± 4.13	1.13 ± 0.22	12.90 ± 1.09	10.19 ± 1.05	4.76 ± 0.67	7.94 ± 0.73	1.60 ± 0.23	0.97 ± 0.19	0.18 ± 0.09	93.82
***L*$_2$, *n* = 10**	71.97 ± 2.57	0.33 ± 0.15	11.01 ± 1.58	2.98 ± 0.93	1.17 ± 0.40	3.20 ± 0.63	2.38 ± 0.28	2.32 ± 0.21	–	95.49
fluid-containing system										
***L*, *n* = 9**	62.26 ± 1.91	1.23 ± 0.08	14.88 ± 0.59	2.68 ± 0.55	5.58 ± 0.52	7.97 ± 0.55	2.33 ± 0.23	1.18 ± 0.10	–	98.12
***L*$_2$, *n* = 10**	76.61 ± 2.07	0.26 ± 0.06	10.62 ± 1.87	0.88 ± 0.33	0.96 ± 0.43	2.17 ± 0.70	2.91 ± 0.50	2.51 ± 0.37	–	96.91

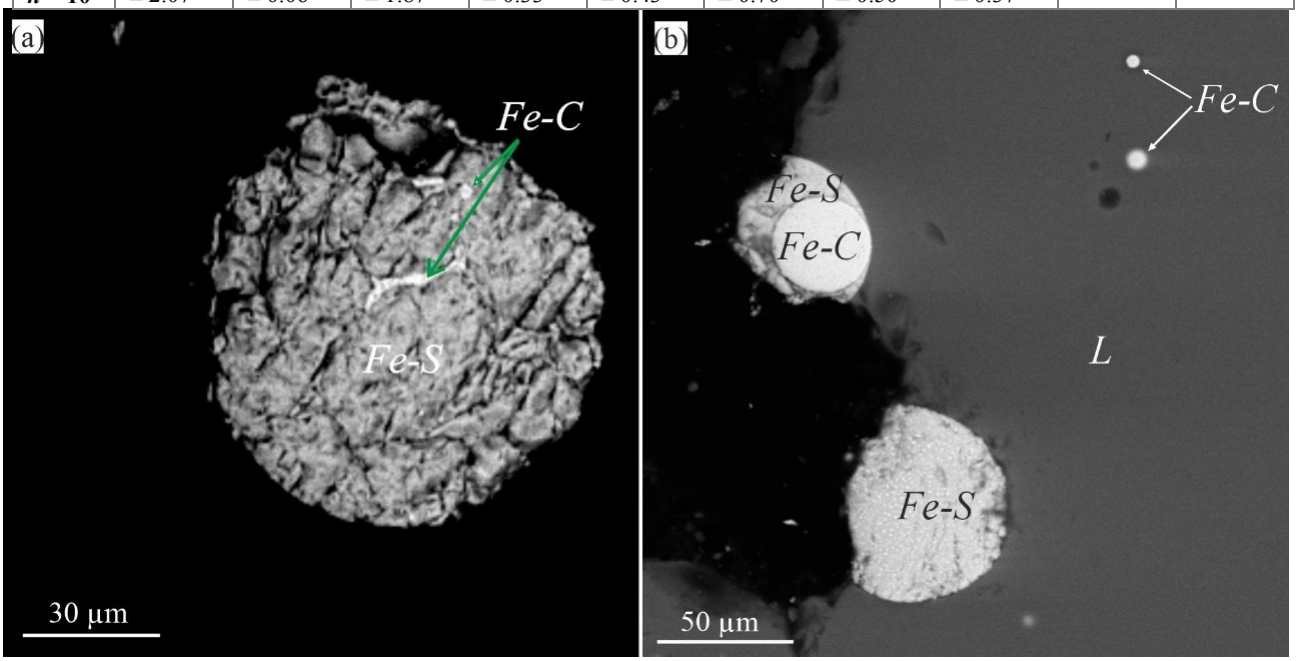

Fig. 2. Backscattered electron micrographs of layered sulfide-metallic phases after experiments in the basalt-sandstone system: a) under dry conditions, b) in the presence of C–O–H–S fluid.

Under fluid-containing conditions, layered sulfide-metal droplets most often formed at the boundary with a graphite container or at the sandstone-basalt boundary. The Fe-C metallic phase has smooth, clear contours (Fig. 2b), reaches 50 μm in size, and contains an average of approximately 89 wt.% Fe. The sulfide phase corresponds to pyrrhotite in Fe and S content, contains approximately 0.6 wt.% Ni, and approximately 0.3 wt.% Cu. In the metallic phase, Ni and Cu are below the detection limit of WDS. Multiple micron-sized homogeneous sulfide droplets are also found in the basaltic melt matrix.

Table 2. Average chemical compositions of sulfide and metallic phases formed during contamination of basalt with sandstone in dry and fluid-containing systems according to WDS analysis (wt.%).

Phase	n	S	Fe	Ni	Cu
dry conditions					
Fe–S	11	33.78 ± 2.59	66.32 ± 1.65	0.32 ± 0.07	–
Fe–C	5	0.74 ± 0.28	94.50 ± 1.25	3.66 ± 0.30	–
fluid-containing system					
Fe–S	14	32.14 ± 3.18	63.61 ± 3.14	0.57 ± 0.28	0.34 ± 0.16
Fe–C	13	0.82 ± 0.21	88.82 ± 5.92	–	–

When basaltic melt was contaminated with pyrite-containing sandstone under dry and fluid-containing conditions, a change in the composition of the basaltic melt, a change in the degree of melting of the sandstone, as well as different conditions for the formation and stratification of the Fe–C–S melt into

Fe-sulfide and Fe-metallic were observed.

The composition of basaltic melt varies from basic basaltic (SiO_2 48 wt.%) to intermediate andesite-basaltic (SiO_2 54 wt.%) under dry conditions, and to acidic alkaline-dacite (SiO_2 64 wt.%) under oil- and gas-saturated conditions. A decrease in MgO concentrations to 5 wt.% under dry conditions, and CaO and TiO_2 concentrations to 8 and 1.2 wt.% in both systems, respectively, is observed. A distinctive feature of the newly formed melts is a significant loss of iron. Compared to the original basalt, where FeO = 14 wt.%, under dry conditions its content drops to 10 wt.%, and in the presence of fluid it does not exceed 2 wt.%. Reduced iron concentrations in silicate melts of the studied systems are primarily associated with the formation of sulfide and metallic melts.

The structural relationships between the sulfide and metallic phases, as well as the form of precipitation, suggest the liquation nature of these formations. The low analysis totals of all Fe-metallic phases (92–96%) indicate carbon dissolution in the metallic melts at levels ranging from 4 to 8 wt%.

Using oil in this study, we wanted to determine whether it would: 1) be a reliable source of hydrocarbon fluid? 2) influence sulfide-silicate segregation? The results obtained provide positive answers to these questions. Oil can also serve not only as a source of hydrocarbon fluid but also as a source of sulfur and, by reacting with iron in the melt, cause the latter's stratification.

Thus, the conducted studies confirm the important role of C–O–H–S fluid in the processes of differentiation of silicate and sulfide melts, as well as the formation of metallic and sulfide ore formation during the interaction of basaltic magmas with oil-and-gas-saturated host rocks.

This study is fulfilled under Research program №FMUF-2022-0001 of the Korzhinskii Institute of Experimental Mineralogy.

References

Barnes S.J., Yudovskaya M.A., Iacono-Marziano G., Vaillant M.L., Schoneveld L.E., Cruden A.R. Role of volatiles in intrusion emplacement and sulfide deposition in the supergiant Norilsk-Talnakh Ni-Cu-PGE ore deposits // Geology. 2023. V. 51. N. 11. P. 1027-1032. https://doi.org/10.1130/G51359.1

Grinenko L.N. Hydrogen sulfide-containing gas deposits as a source of sulfur during sulfurisation of magmas of industrial ore-bearing intrusions of the Norilsk region // Dokl. of the USSR Academy of Sciences. 1984. V. 278. N 3. P. 730-732 (in Russian)

Iacono-Marziano G., Ferraina C., Gaillard F., Di Carlo I., Arndt N.T. Assimilation of sulfate and carbonaceous rocks: Experimental study, thermodynamic modeling and application to the Noril'sk-Talnakh region (Russia) // Ore Geology Reviews. 2017. V. 90. P. 399–413. https://doi.org/10.1016/j.oregeorev.2017.04.027

Kostyuk, A. V., Gorbachev, N. S., Novikov, M. P., Nekrasov, A. N. Experimental Studies of Basaltic Melt Contamination by Sedimentary Rocks // Petrology. 2025. V.33. N6. P. 604-617. DOI: 10.1134/S0869591125700249

Lakhova A. I., C. M. Petrov, V. S. Balitsky, T. V. Setkova, I. N. Plotnikova, L. V. Balitskaya, M. A. Golunova, and T. M. Bublikova. Experimental study of hydrothermal fluid interaction on changes in oil hydrocarbons of different genotypes // Experiment in GeoSciences. 2022. V. 28. N. 1. P. 98–101.

Kuzyura A.V.[1], Spivak A.V.[1], Kriulina G.Yu.[2], Zakharchenko E.S.[1] Ultrabasic diamonds from Zapolyarnaya kimberlite pipe. *UDC 550.4.02, 548.2, 548.5, 549.211*

[1] D.S. Korzhinsky Institute of Experimental Mineralogy of Russian Academy of Science, Russia, Chernogolovka shushkanova@iem.ac.ru spivak@iem.ac.ru egorzero@gmail.com; [2]Lomonosov Moscow State University, Geological Department, Russia, Moscow g9671844057@gmail.com

Abstract. Four diamond crystals from Zapolyarnaya kimberlite pipe of the Yakutian diamond-bearing province, which contain inclusions of magnesiochromites, have been studied using optical microscopy, scanning electron microscopy, color cathodoluminescence imaging, and IR spectroscopy. The internal structure of the diamonds and their relationship with the inclusions indicate that they were formed at conditions of peridotite paragenesis. The cathodoluminescence pattern of the host diamond indicate a multi-stage growth history of the diamond.

***Keywords**: inclusions in diamonds; magnesiochromite; IR-spectroscopy; luminescence; peridotite paragenesis*

Investigation of morphology and inclusions of host diamond allows to reconstruct the crystallization parameters, such as temperature, pressure, and the chemical composition of the diamond-forming parent medium, and their post-growth evolution (Stachel, Harris, 2008).

Modern spectroscopy methods make possible obtaining data on inclusions without violating their integrity, as well as the integrity of the diamond crystal, which gives a new impetus to the study of inclusions in diamonds and makes it especially relevant.

The present work is aimed at studying of peculiarities of diamond crystals with inclusions from Zapolyarnaya kimberlite pipe (Yakutian diamond-bearing province).

Objects and methods. Four diamond crystals from the Zapolyarnaya kimberlite pipe (Yakutsk diamond province) containing inclusions from the

collection of the Geological Faculty of Moscow State University were selected for the study. Two crystals (Zap 3-2 and Zap 3-13) were polished to expose the inclusions appeared on the surface - in the case of 3-2, and one inclusion - in the case of 3-13. Inclusions in crystal Zap-2-3 have been brought to the surface by a technogenic fracture. In sample Zap 5-7, differently oriented inclusions are located within the host crystal close to the surface (Fig. 1). Previously (Groza et al, 2025), Raman spectroscopy combined with SEM and EMP data, identified the majority of inclusions in the studied diamond crystals (Zap-2-3, Zap-3-13, Zap-5-7) as magnesiochromites. Among the identified by Raman-spectroscopy mineral phases of inclusions inside the crystal Zap-3-2, dominant phase was garnet, with other minerals including rutile, carbonates such as calcite and magnesite, pyroxenes such as omphacite and diopside, and sometimes in association with calcite, magnesiochromite inclusions were present as well, and they were brought out on the surface by grinding.

Chromespinel, along with chromian pyrope and olivine, is one of the main inclusions in diamonds of ultrabasic paragenesis (Sobolev, 1977).

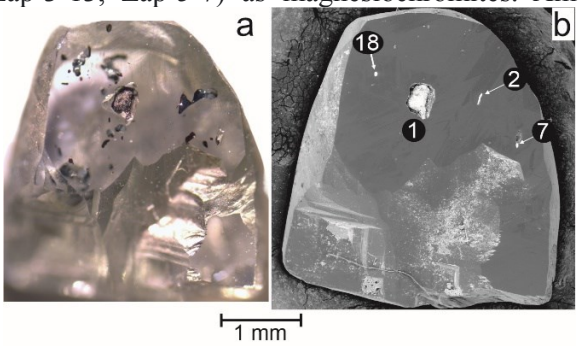

Fig. 1. Optical (a) and SEM (b) images of the diamond crystal Zap 3-2 with magnesiochromite inclusions

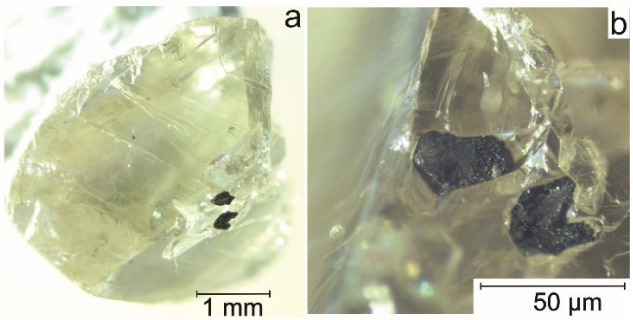

Fig. 2. Optical images of the whole diamond crystal Zap 2-3 with magnesiochromite inclusions (a) and magnified area with the inclusions (b)

The morphology and optical characteristics of diamonds and inclusions were studied using an ADF STD16 binocular microscope and a Nikon Eclipse LV100Npol polarizing microscope.

Infrared spectra were recorded on a "Vertex-70" Fourier spectrometer (Bruker) with a "Hyperion-1000" microscope. Integral (whole crystal volume) absorption spectra in the range (5000 - 500 cm^{-1}) were acquired. The presence of A, B_1, and B_2 defects in the diamonds was determined from the spectra, and their concentrations were calculated. The total nitrogen (Ntot) was determined by summing the detected concentrations of this impurity in the A- and B- forms. Spectra normalization was performed based on absorption in the two-phonon region (Dishler, 2012). The total nitrogen concentration (Ntot) and the fraction of nitrogen in the defect form (% B) were calculated using known proportionality coefficients. The presence and relative content of hydrogen-containing centers were determined in accordance with (Goss et al., 2014).

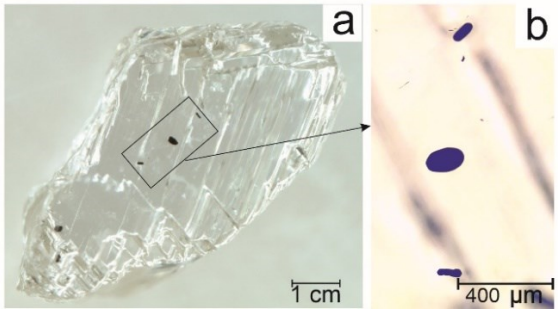

Fig. 3. Optical image of the whole diamond crystal (a) and magnified area with magnesiochromite inclusion (b)

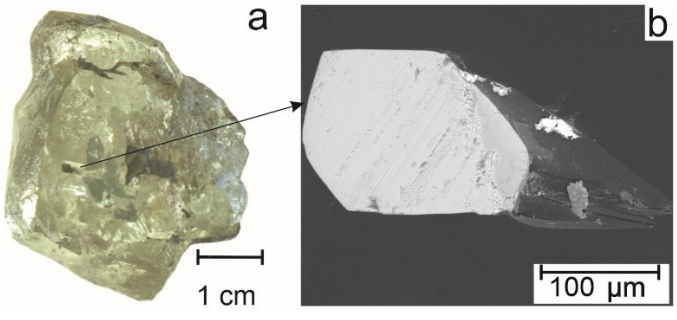

Fig. 4. Optical image of the whole diamond crystal (a) and SEM image of magnesiochromite inclusion (b)

The photoluminescence spectra were obtained using an Aurora Diamond Inspector S1 device at liquid nitrogen temperature (~77 K) with an excitation wavelength of 365 nm.

Cathodoluminescent images were captured on a Cameca MS-46 microprobe analyzer fitted with a high-resolution Videoscan-285 Camera and an Ocean Optics USB2000 + VisNIR-ES spectrometer, which

allows obtaining cathodoluminescence images in natural colors (Novikov et al., 2017). The images were taken at an accelerating voltage of 20 kV and a beam current of 20 nA at room temperature at the IFPH RAS.

Results

Defect-Impurity Composition. According to IR spectroscopy data, studying diamond crystals with magnesiochromite inclusions are classified as type IaAB. Peaks in the two-phonon region (2282 and 2500 cm^{-1}) are associated with diamond lattice absorption, while those in the one-phonon region are related to the presence of structural-impurity defects. Absorption peaks at 1282 cm^{-1} (A-center), 1175 cm^{-1} (B_1-center), and 1362 cm^{-1} (B_2-center) are clearly detected in the spectra (fig. 5).

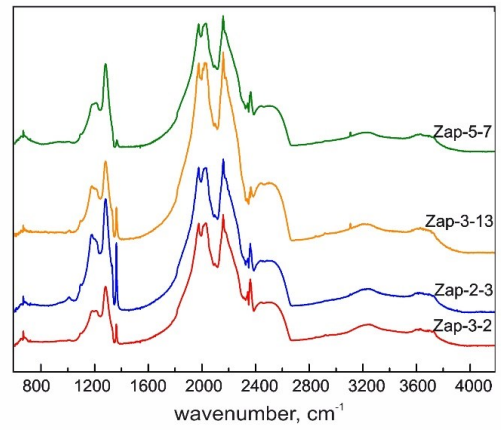

Fig. 5. Infrared (IR) spectra of the diamonds.

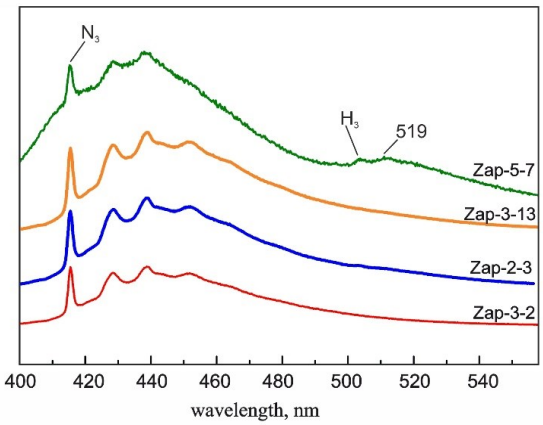

Fig. 6. Photoluminescence (PL) spectra of the diamonds: a) crystal Zap-3-2; b) crystal Zap-2-3; c) crystal Zap-3-13; d) crystal Zap-5-7

	A, at. ppm	B, at. ppm	N_{tot}, at. ppm	B, %	Absorption 3107 cm^{-1}	Max position, B_2, cm^{-1}	Absorption coefficient B_2, cm^{-1}
Zap-2-3	150	110	260	34	0,2	1362	5,3
Zap-3-2	192	58	250	23	0,2	1362	0,0
Zap-3-13	85	55	140	37	0,4	1362	2,0
Zap-5-7	130	40	170	20	0,4	1365	0,7

Concentration calculations indicate that these diamonds are low-nitrogen (Ntotal = 140-260 at. ppm) with a low B-form nitrogen aggregation percentage (% B = 20-37%) (Table 1).

According to (Taylor, Milledge, 1995), such IR-characteristics are typical of crystals from an ultrabasic paragenesis. The presumed calculated formation temperature for these crystals is the highest, corresponding to 1250-1300 °C. B_2-centers (platelets) have been observed in these diamonds. The position of the absorption maximum for this center at 1362-1365 cm^{-1} also indicates high diamond formation temperatures, while their extremely low relative content is consistent with a low nitrogen content in the diamond structure.

Luminescence. All investigated diamonds exhibit blue luminescence when excited at 365 nm (Fig. 6). The main defect of all the diamonds is the N3 centers (3N+V), with zero-phonon line at 415. Crystal Zap-5-7 displays an additional H3 peak.

Cathodoluminescence (CL) images reveal growth zonation of the crystals (Fig. 7 b, d, e). This rectilinear banding is characteristic of octahedral growth sectors. The CL patterns show the relationship between the inclusions and the host diamond: the shape of the inclusion minerals, both isometric and elongated irregular formations, most likely indicates that the diversity is due to the co-growth of diamond and chromite.

Fig. 8a-b clearly illustrates how the rectilinear octahedral zoning of the central and intermediate zones of the Zap-3-2 crystal is interrupted closer to the peripheral zone, leading to the re-crystallization (possibly due to oxidative dissolution) of the diamond into a dodecahedroid. Around the magnesiochromite inclusion, the parallel bands are interrupted, demonstrating layered growth of the diamond, which indicates the syngenetic nature of the inclusion and the diamond. However, there is a small cavity around the inclusion, and the surface of the magnesiochromite is chemically heterogeneous. This likely indicates a reduction in the inclusion's volume during crystallization and/or the presence of a fluid in equilibrium with magnesiochromite, which has partially dissolved the chromite grain surface.

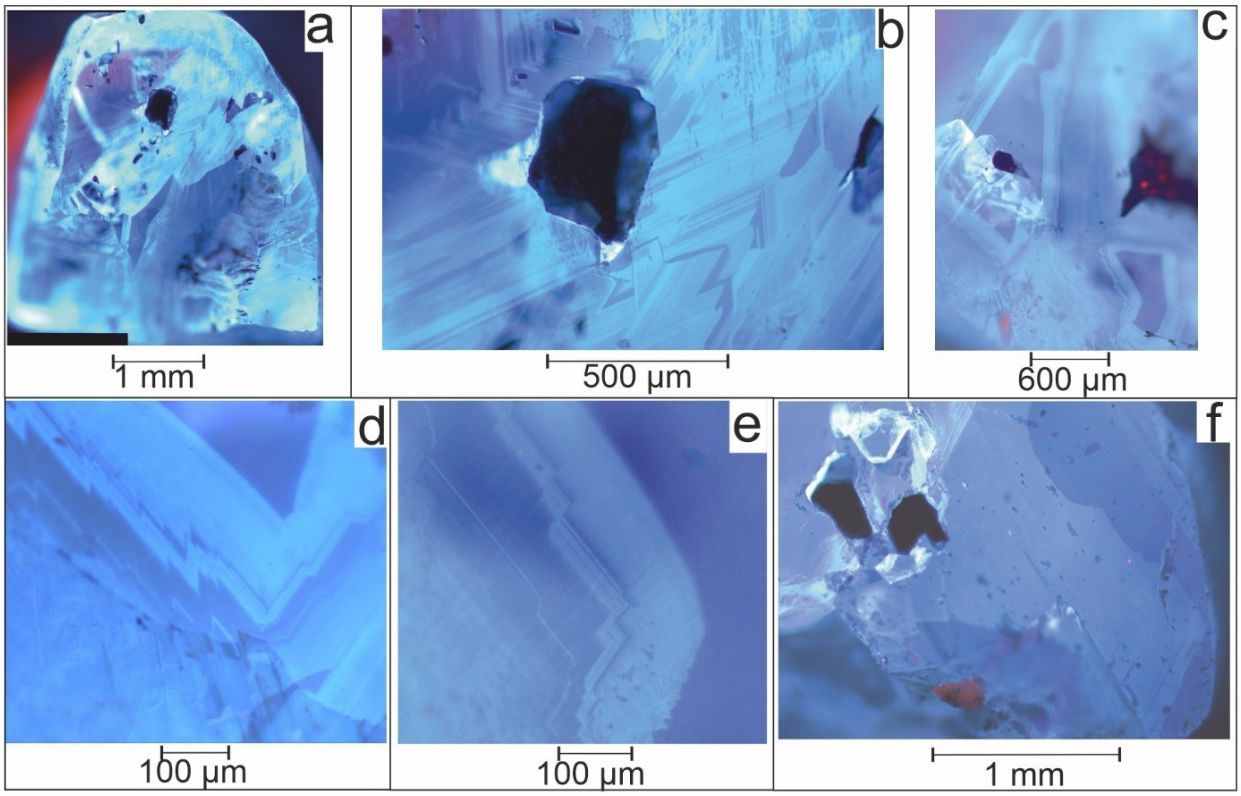

Fig. 7. Color cathodoluminescence images of studied crystals with magnesiochromite inclusions: a) whole crystal Zap 3-2 and b) the inclusion of magnesiochromite mainly in it; c) Zap 3-13 crystal area, two diamond embryos, one of which contains a magnesiochromite inclusion at its center; d) plastic deformations in crystal Zap-3-2; e) plastic deformations in crystal Zap-3-13; f) Zap 5-7 crystal area with the inclusions**.**

The image of Zap 3-13 crystal (Fig. 7c) shows 2 diamond seeds. In the center of one of them, there is a magnesiochromite inclusion. The zone around the inclusion is homogeneous, however, the seed itself (essentially a diamond within a diamond) is contrasting in the image, and therefore, having a different nitrogen center content, is protogenetic to the host diamond. This is a clear demonstration of the multistage nature of diamond formation and the different temporal relationship between the diamond-inclusion and the host diamond.

Conclusions

Therefore, four diamond crystals from Zapolyarnaya kimberlite pipe with inclusions of magnesiochromite using spectroscopy and luminescence methods demonstrated that these diamonds were formed at conditions of ultrabasic paragenesis at temperatures 1250 -1300 °C. All diamonds have a low nitrogen content (up to 260 ppm of N_{tot}) in the diamond structure; inclusions are paragenetic to their host crystals, excluding crystal Zap 3-13, which is protogenetic to the host diamond.

Funding The work was fulfilled under Research program № FMUF-2022-0001 of the D.S. Korzhinskii Institute of Experimental Mineralogy of Russian Academy of Science as well as within the Government assignment of M. V. Lomonosov Moscow State University, on the state budget topic "Mineralogical study of deposits in the Arctic zone of Russia with the aim of their comprehensive development (state registration 121061600049-4)

Gratitude

We express our gratitude to Dr. of Chemical Sciences, Professor of the Russian Academy of Sciences A.A. Shiryaev for cathodoluminescence imaging and interpreting the obtained data.

References

Stachel, T. & Harris, J. W. The origin of cratonic diamonds - Constraints from mineral inclusions // Ore Geol. Rev. — 2008. — V.34, — p. 5–32.

Groza V.S., A.V. Kuzyura, A.V. Spivak, G.Yu. Kriulina, E.S. Zakharchenko, A.V. Kuzmin, A.V. Skryabina. Peculiarities of Magnesiochromite Compositions from Inclusions in Diamonds of the Zapolyarnaya Kimberlite Pipe (Yakutia) / Proceedings of the XVI all-Russian school for young scientists "Experimental mineralogy, petrology, and geochemistry". October 20-21, — 2025. Chernogolovka. — p. 31-36.

Sobolev N.V. Deep Seated Inclusions in Kimberlites and Composition of the Upper Mantle. —Washington DC: American Geophysical Union, 1977. —279 p.

Dishler B. Handbook of Spectral Lines in Diamond. — Springer: Dudar V.A., North Timan placers, Ores and metals. 2012. —467 p.

Goss J.P., Briddon P.R., Hill V., Jones R., Rayson M.J. Identification of the structure of the 3107 cm^{-1} H-related defect in diamond // J. Phys.: Condens. Matter. — 2014. — V. 26. — P. 1–6. DOI:10.1088/0953-8984/26/14/145801

Novikov I., Griboedova, Golovanova T. Interpretation of Cathodoluminescence Patterns on the Example of Fluorapatite from the Konder Massif (Aldan) //Analytics. — 2017. —V. 1/ (32) (in Russian).

Taylor, W., & Milledge. H.J. Nitrogen aggregation character, thermal history and stable isotope composition of some xenolith-derived diamonds from Roberts Victor and Finsch // International Kimberlite Conference: Extended Abstracts. — 1995, — V. 6(1), — p. 620–622. https://doi.org/10.29173/ikc1988

Levshunova S.P.[1], Kartashov A.A.[1], Ivanova S.R.[1] Geothermal conditions of oil generation at great depths under harsh thermobaric conditions. *UDC 553.98*

[1] – FSBI "VNIGNI", Moscow lev@vnigni.ru

Abstract. The mechanism of secondary oil formation at great depths is considered, resulting from the contact of paleo-pools of hypergenically altered oils and paleobitumens with a mixture of carbon dioxide and water vapor, which has a high dissolving capacity with respect to hydrocarbons, resins, and asphaltenes under conditions of high temperatures and pressures. Such a formation mechanism is demonstrated for accumulations of liquid hydrocarbons in the Upper Devonian deposits of well 2 Volodarskaya in the Caspian Basin at a depth of 5961 m.

Keywords: *oil, great depths, high temperatures, high pressures, Caspian Basin*

According to the existing concept of the zonation of catagenetic transformation of organic matter in rocks, gas accumulations are expected to be discovered in the lower horizons of the sedimentary cover of the Earth's crust. At the same time, there is evidence, particularly from foreign territories composed of carbonate formations, of the widespread occurrence of oils at great depths. Moreover, these oils are characterized by specific features: they have a high density, reaching 0.88–0.90 g/cm³ even at depths exceeding 4.9 km. In the Maracaibo, Western Canadian, and Southeastern Mexico oil basins, at great depths (over 5 km) under harsh thermobaric conditions, practically within the Main Zone of Gas Formation, heavier and heavy oils (0.87–0.92 g/cm³) have been discovered (Vysotsky, Guseva, 1977).

At great depths, in the zone of high temperatures (exceeding 80°C), carbonate sequences undergo hydrolysis, leading to the formation of large amounts of carbon dioxide. Indeed, in the gases of ancient platforms at great depths, a high CO_2 content is observed. For example, within the North American Platform in the Permian Basin, at the Mi-Vida field in the Ellenburger carbonate formation at a depth of 5533 m, the CO_2 concentration reaches up to 52%. Within the East European Platform, in the Pre-Caspian Depression, in the Paleozoic sub-salt carbonate formations of the Astrakhan Arch, its concentrations rise to 20% and higher, increasing both downward in the section and in the southwestern direction toward the Karakul-Smyshkovo zone, reaching 84–97%.

In Well 2 Volodarskaya (Astrakhan Arch), from a depth of 5961 m, heavy oil with a density of 0.871 g/cm³ was obtained from carbonate deposits of Upper Devonian–Lower Carboniferous age. To the south, from the same deposits within the Karakul-Smyshkovo zone of uplifts, in Well 1 Krasnokhudukskaya, under even more severe thermobaric conditions (reservoir temperature 180°C), formation water with oil films was obtained. The type of organic matter was determined as sapropelic. The stage of catagenetic transformation is very high: MK 3–4 – AK. Using the authors' original method, very high concentrations (exceeding 100 cm³/kg) of dry hydrocarbon gases (CH_4 over 90%) sorbed by the rocks were extracted from the rock powder under vacuum. These data indicate that the organic matter of the Upper Devonian–Lower Carboniferous formations is located in the Main Zone of Gas Formation. Nevertheless, heavy oil was discovered here (Levshunova, 2001, 2004).

Research on the solubility of high-boiling hydrocarbons in compressed gases in our country began as early as the 1950s. Particular attention was paid to the dissolving capacity of CO_2. A synthesis of the results obtained from these experiments allows us to draw the following conclusions. It has been established that at temperatures around 100°C and pressures of 80 MPa, hydrocarbons up to C14–C15 inclusive dissolve in carbon dioxide. As temperatures rise to 400°C and pressures to 120 MPa, all components (including resins and asphaltenes) dissolve in carbon dioxide, forming heavy secondary oils (Zhuze, 1977, 1981; Petrenko et al., 1997).

Oils from deep horizons of the Pre-Caspian Depression likely have a similar genesis, both within the Astrakhan Arch (Volodarskaya Well 2, Upper Devonian, 5.8–5.9 km, oil density 0.8717 g/cm³) and in the Kazakhstani sector of the Pre-Caspian Depression (Karachaganak field, Upper Devonian, deeper than 5 km, oil density 0.88–0.92 g/cm³). The oils from Devonian deposits in oil-and-gas shows within the Karakul-Smyshkovo zone of uplifts have the same genesis. Here, in the upper parts of the Lower Carboniferous deposits, where the severity of thermobaric conditions decreases, semi-viscous

bitumens are present (Petsyukha, Anisimov, 1977). Increasingly severe thermobaric conditions lead to the appearance of heavy oil films in the Upper Devonian deposits.

Thus, a method is proposed for predicting the phase state of hydrocarbons not only based on the traditional zonation of catagenetic transformation of organic matter in rocks, but also taking into account specific transformations in the presence of carbon dioxide sources. This expands the range for discovering oils at great depths, including secondary oils resulting from the dissolution of paleobitumens in carbon dioxide. The presence of condensed water vapor enhances this process.

The work was carried out within the framework of the State Assignment of the Federal State Budgetary Institution "VNIGNI" No. 049-0000-23-00 dated 12/30/2022 and No. 049-00016-24-00 dated 12/29/2023.

References

1. Zhuze, T.P. (1974). Compressed Gases as Solvents. Moscow: Nedra, 111 p.
2. Zhuze, T.P. (1981). The Role of Compressed Gases as Solvents. Moscow: Nedra, p. 165.
3. Levshunova, S.P. (2001). Genesis of Heavy Oils in Carbonate Deposits. Oil and Gas Geology, No. 1, pp. 6-10.
4. Levshunova, S.P. (2004). Non-Hydrocarbon Gases and Their Role in Oil Formation. Moscow: Sputnik, 99 p.
5. Vysotsky, V.I., & Guseva, A.N. (Eds.). (1977). Oils and Gases of Foreign Fields: A Handbook. Moscow: Nedra, 327 p.
6. Petrenko, V.L., Shuganov, V.D., Petrenko, N.V., & Beletskaya, S.N. (1997). Mechanism of Transformation of Liquid and Gaseous Hydrocarbons. In XVIII International Congress on Organic Geochemistry: Abstracts. Maastricht, pp. 160-170.
7. Petsyukha, Yu.A., & Anisimov, L.A. (1977). Abnormally High Pressures in Paleozoic Deposits of the Western Marginal Zone of the Pre-Caspian Depression. Oil and Gas Geology, No. 5, pp. 48-53.